ENVIRONMENTAL RESEARCH
LETTERS

LETTER • OPEN ACCESS

Solar radiation variation weakened the boost of gross primary production by vegetation restoration in China's most forestry engineering areas during 2001–2020

To cite this article: Yanlian Zhou *et al* 2024 *Environ. Res. Lett.* **19** 014082

ENVIRONMENTAL RESEARCH
LETTERS

CrossMark

OPEN ACCESS

RECEIVED
16 August 2023

REVISED
13 December 2023

ACCEPTED FOR PUBLICATION
3 January 2024

PUBLISHED
11 January 2024

LETTER

Solar radiation variation weakened the boost of gross primary production by vegetation restoration in China's most forestry engineering areas during 2001–2020

Yanlian Zhou[1,5], Xiaonan Wei[1], Yuyan Wang[1], Wei He[1,2,*], Zhoutong Dong[1], Xiaoyu Zhang[1], Yibo Liu[3], Ngoc Tu Nguyen[4] and Weimin Ju[2,5]

[1] Jiangsu Provincial Key Laboratory of Geographic Information Science and Technology, Key Laboratory for Land Satellite Remote Sensing Applications of Ministry of Natural Resources, School of Geography and Ocean Science, Nanjing University, Nanjing, Jiangsu 210023, People's Republic of China
[2] International Institute for Earth System Science, Nanjing University, Nanjing 210023, People's Republic of China
[3] Jiangsu Laboratory of Agricultural Meteorology, Institute of Ecology, School of Applied Meteorology, Nanjing University of Information Science & Technology, Nanjing 210044, People's Republic of China
[4] State Key Laboratory of Hydrology-Water Resources and Hydraulic Engineering, College of Hydrology and Water Resources, Hohai University, Nanjing, People's Republic of China
[5] Jiangsu Center for Collaborative Innovation in Geographic Information Resource Development and Application, Nanjing, Jiangsu 210023, People's Republic of China
[*] Author to whom any correspondence should be addressed.

E-mail: weihe@nju.edu.cn

Keywords: gross primary production, land cover change, CO_2 fertilization, climate change, TL-LUE model, forestry engineering areas of China

Supplementary material for this article is available online

Abstract

Over the past decades, ecological restoration initiatives in China have made great progress in restoring degraded forests and increasing vegetation coverage, yet the carbon sequestration effects of these initiatives in the context of climate change are not clear. In this study, we assessed the effects of vegetation restoration on gross primary production (GPP) in China's forestry engineering areas, where large-scale vegetation restoration programmes were launched, during 2001–2020 by disentangling the respective roles of land cover change (LCC), CO_2 fertilization, and climate changes using a two-leaf light use efficiency model. We found that LCC attributed by the vegetation restoration dominantly accelerated the increase of GPP in seven out of the eight areas, and CO_2 fertilization played a near-equivalent role in all areas. By contrast, the changes in different climate factors contributed to GPP variations diversely. The solar radiation variation greatly inhibited the vegetation GPP over time in seven out of these areas, and the changes in air temperature and vapor pressure deficit regulated GPP inter-annual variations without clear trends in all areas. This study advances our understanding of the contribution of China's afforestation on its forest GPP in a changing climate, which may help to better manage forests to tackle the challenge of the climate crisis in the future.

1. Introduction

Terrestrial gross primary production (GPP), as the largest component of the global terrestrial carbon budget, plays an important role in the global carbon cycle (Ichii *et al* 2005, Zhao *et al* 2005, Piao *et al* 2009, Ahlström *et al* 2015). GPP is vulnerable to changes in climate and atmospheric CO_2 concentration and disturbances from human activities (Friedlingstein *et al* 2010, Li *et al* 2015). Thus, it is of great importance to investigate the fate of regional GPP in a changing climate with human interferences.

The changing climate and the rising atmospheric CO_2 concentration affect vegetation growth and carbon cycle strongly. They alter the physiological constraints on plant photosynthetic rates (Nemani *et al* 2003, Zhao and Running 2010, Piao *et al* 2013, Chen *et al* 2019). The increase in CO_2 concentration increases the intercellular CO_2 content and thus promotes leaf photosynthesis (Piao *et al* 2013, Jiang and Ryu 2016, Chen *et al* 2019). Solar radiation (Rad) is considered to be the main driver of the negative effect of global GPP from 1982 to 2015 (Sun *et al* 2018). Warming further reduces the pressure of air temperature (Ta) to increase GPP in the northern high latitude cold regions (Nemani *et al* 2003), while increasing Ta can increase vapor pressure deficit (VPD) and thus exacerbate drought stress (Liu *et al* 2019), leading to a decrease in GPP (Ciais *et al* 2005, Zhao and Running 2010, Anderegg *et al* 2015).

In the late 20th century, the Chinese government launched large-scale vegetation restoration programmes, including the Global Canopy Program and natural forest conservation projects, to mitigate land degradation, desertification and soil erosions (Yang *et al* 2014, Li 2021). Through these projects, vegetation cover on land surface has increased significantly, effectively limited soil erosion (Xin *et al* 2011, Liu *et al* 2012a, Sun *et al* 2015) and contributed significantly to regional and global carbon sinks (Guo *et al* 2013, Fang *et al* 2014, Li *et al* 2015, Xiao *et al* 2015). The Three-North Shelter Forest Program, initiated in 1978 (Zhang *et al* 2016), has contributed to an increase of 8.05% in forest cover and a slight increase in GPP (Xie *et al* 2020). The Pearl River Shelter Forest Program has brought significant changes in forest cover since 1996 (Hasan *et al* 2019, Xiao *et al* 2019) and land cover change has become the main contributor to forest GPP increase since 2011 (Zhang *et al* 2022). The forestry engineering areas in China have different climate change characteristics (Yang *et al* 2014, Li 2021), GPP could be affected differently by LCC, CO_2 and climate change in individual ecological areas, but existing studies are often incomplete in the consideration of impacting factors with empirical attribution frameworks (e.g. by linear regressions), hampering our understanding on the capacity of vegetation to sequester carbon. Thus, a systematic understanding of the effects of China's vegetation restoration initiatives over time in the context of changing climate is urgently needed.

In this study, we assess the effects of the vegetation restoration on GPP in China's forestry engineering areas during 2001–2020 by disentangling the respective roles LCC, CO_2 fertilization, and climate changes using a two-leaf light use efficiency (TL-LUE) model with scenario simulations. The objectives of this study are: (1) to characterize the dynamic of the GPP in eight forestry engineering areas with different vegetation types since 2001; (2) to disentangle and quantify the individual and combined effects of changes in LCC, CO_2 and climate factors (Rad, Ta and VPD) on the GPP of eight forestry areas in China.

2. Data and method

2.1. Data

2.1.1. Remote sensing data

Land cover data were obtained from the MODIS Land Cover product MCD12Q1 v006 dataset (https://lpdaac.usgs.gov/products/mcd12q1v006/) with an annual temporal resolution and a spatial resolution of 500 m × 500 m (Sulla-Menashe *et al* 2019) from 2001–2020 with the International Geosphere-Biosphere Programme classification system. Leaf area index (LAI) data from GlobMap LAI version V3 for 2001–2020 were obtained by inversion of MODIS surface reflectance data (Deng *et al* 2006, Liu *et al* 2012b) with a temporal resolution of 8 d and a spatial resolution of 500 m × 500 m. The long-term LAI was compared with field measurements, showing an error of 0.81 on average (Liu *et al* 2012b).

2.1.2. Meteorological and CO_2 concentration data

The daily meteorological data were interpolated from 753 meteorological stations across the country for the period of 2001–2020 with a spatial resolution of 500 m × 500 m. The climate variables include solar radiation (Rad), air temperature (Ta) and relative humidity. Both daily Rad and daily Ta are in good agreement with the tower observations, and Ta showed high agreement with the 0.5° monthly air temperature data from the China Meteorological Administration (http://cdc.cma.gov.cn) (Liu *et al* 2016).

Monthly CO_2 concentration was used in the simulation which was obtained from direct measurements at the Mauna Loa Observatory in Hawaii (https://gml.noaa.gov/ccgg/trends) calculated from hourly observations.

2.1.3. Study area

The spatial distribution and specific information of the eight areas in China (www.resdc.cn/data.aspx?DATAID=138) are shown in figure 1 and table 1.

2.1.4. Flux data for model validation

To test the performance of TL-LUE model in simulating GPP (GPP_TL), the model was validated at both site and regional scales. At site scale, monthly GPP data from 12 sites (91 site years) of ChinaFlux were selected, including 4 forest sites, 2 wetland sites, 5 grassland sites, and 1 cropland site (supplementary table 1).

To assess the performance of the TL-LUE model to simulate GPP at a regional scale, FluxSat GPP (https://avdc.gsfc.nasa.gov/pub/tmp/FluxSat_GPP/, Schaaf *et al* (2002)) and GOSIF GPP (http://globalecology.unh.edu/data/GOSIF-GPP.html, Li and Xiao (2019)) during the period 2001–2020 were

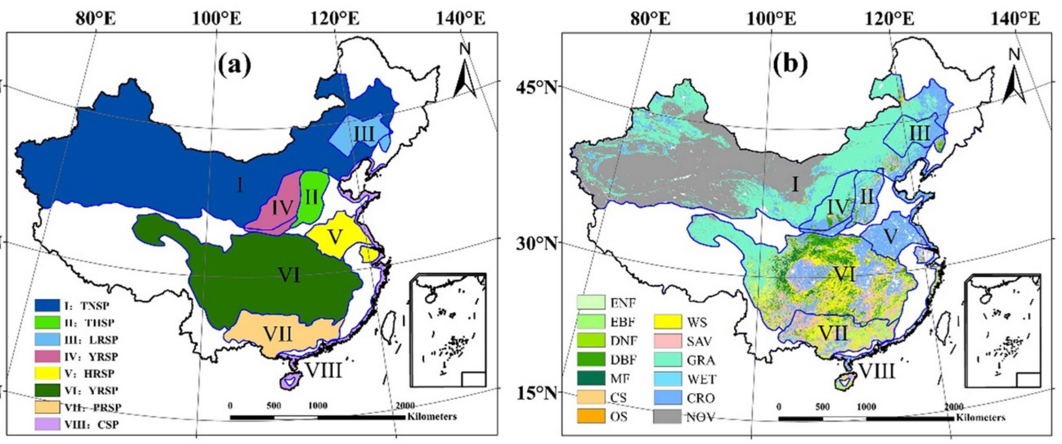

Figure 1. Spatial distribution of eight forestry engineering areas (a). I is the Three-north shelterbelt program (TNSP), II is the afforestation program for Taihang mountain (THSP), III is shelterbelt program for Liaohe river (LRSP), IV is the shelterbelt program for middle reaches of Yellow river (YRSP), V is shelterbelt program for Huaihe river and Taihu lake (HRSP), VI is shelterbelt program for upper and middle reaches of Yangtze river (YRSP), VII is shelterbelt program for Pearl river (PRSP), VIII is coastal shelterbelt program (CSP). Land cover data of from MCD12Q1 v006 in eight areas in 2020 (b). ENF, EBF, DNF, MF, CS, OS, WS, SAV, GRA, WET, CRO and NOV means evergreen needle leaf forest, evergreen broadleaf forest, deciduous needle leaf forest, mixed forest, open shrubland, woody savannas, savannas, wet, cropland, grassland, non-vegetation, respectively.

Table 1. Information of eight forestry engineering areas.

Area	Name	Lon (°)	Lat (°)	Area ($\times$10 000 km^2)	Startup Time
I	Three-north shelterbelt program (TNSP)	69.95°–128.83°E	31.65°–50.85°N	261.06	1978
II	Afforestation program for Taihang mountain(THSP)	110.59°–116.48°E	34.55°–40.95°N	13.03	1986
III	Shelterbelt program for Liaohe river (LRSP)	116.51°–126.29°E	40.70°–46.23°N	16.91	1994
IV	Shelterbelt program for middle reaches of Yellow river(YRSP)	104.73°–112.89°E	33.99°–40.89°N	18.47	1996
V	Shelterbelt program for Huaihe river and Taihu lake(HRSP)	112.17°–122.21°E	30.39°–36.53°N	17.72	1997
VI	Shelterbelt program for upper and middle reaches of Yangtze river(YRSP)	90.35°–120.06°E	23.76°–36.46°N	120.15	1989
VII	Shelterbelt program for Pearl river(PRSP)	102.39°–116.31°E	21.01°–26.71°N	28.12	1996
VIII	Coastal shelterbelt program(CSP)	108.09°–124.76°E	17.12°–42.13°N	15.41	1990

used. They have been shown to have high accuracy in GPP estimation and are widely used in carbon cycle studies (Joiner *et al* 2018, Li and Xiao 2019, Bai *et al* 2021, Byrne *et al* 2021). In this study, FluxSat GPP and GOSIF GPP datasets with a spatial resolution of 0.05° $\times$ 0.05° were accumulated to a monthly scale and resampled to 500 m $\times$ 500 m. Although no direct item was used to describe the impacts of CO_2 fertilization effects, the FluxSat and GOSIF GPP data were derived directly from flux and SIF observations (data-driven), respectively, which indirectly reflect the CO_2 fertilization effects on vegetation through vegetation variables.

2.2. Method

2.2.1. TL-LUE model

The latest version of the TL-LUE model (Bi *et al* 2022) simulates GPP as follows:

$$\mathrm{GPP} = (\varepsilon_{\mathrm{msu}} \times \mathrm{APAR_{su}} + \varepsilon_{\mathrm{msh}} \times \mathrm{APAR_{sh}}) \times f(\mathrm{VPD}) \times g(\mathrm{Ta}) \times c(\mathrm{CO_2}) \quad (1)$$

where $\varepsilon_{\mathrm{msu}}$ and $\varepsilon_{\mathrm{msh}}$ denote the maximum LUE of sunlit and shaded leaves in the vegetation canopy, respectively; $f(\mathrm{VPD})$, g (Ta) and $c(\mathrm{CO_2})$ were regulation scalars of VPD, Ta and atmospheric CO_2 concentration, respectively, which were described in

Table 2. Scenario simulations.

Scenario simulation	Land cover + LAI	CO_2	Rad	Ta	VPD
I	2001–2020	2001–2020	2001–2020	2001–2020	2001–2020
II	2001	2001–2020	2001–2020	2001–2020	2001–2020
III	2001–2020	2001	2001–2020	2001–2020	2001–2020
IV	2001–2020	2001–2020	2001	2001–2020	2001–2020
V	2001–2020	2001–2020	2001–2020	2001	2001–2020
VI	2001–2020	2001–2020	2001–2020	2001–2020	2001

Bi *et al* (2022) and Zhou *et al* (2016); $APAR_{su}$ and $APAR_{sh}$ are the PAR absorbed by sunlit and shaded leaves, respectively, which were calculated as:

$$APAR_{su} = (1-\alpha)\times\left[PAR_{dir}\times\frac{\cos\beta}{\cos\theta} + \frac{PAR_{dif}-PAR_{dif,u}}{LAI}+C\right]\times LAI_{su} \quad (2)$$

$$APAR_{sh} = (1-\alpha)\times\left[\frac{\left(PAR_{dif}-PAR_{dif,u}\right)}{LAI}+C\right]\times LAI_{sh} \quad (3)$$

where α denotes albedo, which varies among vegetation types; β is the leaf inclination angle (60°); θ is the solar zenith angle; C denotes the multiple scattering term of Rad inside the vegetation canopy; $PAR_{dif,\,u}$ is the scattered Rad below the vegetation canopy; PAR_{dir} and PAR_{dif} are the direct solar Rad and scattered Rad. The calculation of C, PAR_{dif}, u, PAR_{dir}, PAR_{dif}, and R refers to He *et al* (2013), Zhou *et al* (2016) and Bi *et al* (2022). As for scaling from hourly scale to daily scale, we followed the method by Chen *et al* (1999). Firstly daily averaged solar declination was calculated, then daily averaged solar zenith angle was calculated, and finally daily averaged PARdir and PARdif were calculated according to equations (2) and (3).

2.2.2. Simulation setup

Six scenarios were simulated to quantify the impact of changes in LCC, CO_2 and meteorological factors on GPP over the period of 2001–2020 (table 2).

In Scenario I, the TL-LUE model was driven by the observed data of land cover, LAI, CO_2 and meteorological factors (Rad, VPD and Ta) that followed the historical changes or the period of 2001–2020 to simulate GPP.

In Scenario II, the TL-LUE model was driven by the same datasets of CO_2 and meteorological factors (Rad, VPD and Ta) as in Scenario I, except the land cover and LAI dataset. The land cover and LAI data are kept at 2001 levels.

In Scenario III, the same datasets of land cover, LAI and meteorological factors (Rad, VPD and Ta) as in Scenario I, and CO_2 in 2001 was used to drive the TL-LUE model to explore the effects of CO_2 changes on vegetation GPP after 2001.

In Scenario IV, the same land cover, LAI, CO_2, Ta and VPD datasets as in Scenario I, except Rad, which is kept at 2001 levels to analyze the effect of Rad changes on vegetation GPP over two decades.

In Scenario V, the same land cover, LAI, CO_2, Rad and VPD data sets were used as in Simulation I, except Ta, which is kept in 2001 to analyze the effect of Ta changes on vegetation GPP over the last 20 years.

In Scenario VI, the same land cover, LAI, CO_2, Rad and Ta data sets were used as in Simulation I, except VPD, which is kept in 2001 to analyze the effect of VPD changes on vegetation GPP over the last 20 years.

2.2.3. Calculating the effects and cumulative effects of impact factors on GPP

The differences between dynamic and static simulations on vegetation GPP was used according to the equation:

$$\Delta GPP = GPP_{Dynamic} - GPP_{Static} \quad (4)$$

where $GPP\_{}_{Dynamic}$ is the GPP in Scenario I, $GPP\_{}_{Static}$ is the GPP results from Scenarios II–VI, and ΔGPP is the dynamic effect of changes in LCC, CO_2, Rad, Ta and VPD on vegetation GPP, respectively.

The cumulative impact of each factor on GPP is expressed as:

$$\text{Cumulative\_}\Delta GPP = \sum_{2001}^{j}\sum_{i}\Delta GPP \quad (5)$$

where j is the year ranging from 2001 to 2020; i was the the ith pixel.

3. Results

3.1. Model validation and evaluation

The site-scale validation showed that TL-LUE model was able to track the seasonal and inter-annual variations of GPP (figure 2). The R^2 ranged 0.67–0.96 for the 12 sites. We also evaluated our simulation with two other GPP products (GPP_Fluxsat and GPP_GOSIF) at the regional scale (supplementary figure S1). 98.57% of the vegetation areas had a significant positive correlation between monthly GPP_TL and GPP_Fluxsat ($p < 0.05$) with an average R^2 of 0.78. And monthly GPP_TL was significantly positively correlated with GPP_GOSIF ($p < 0.05$) with

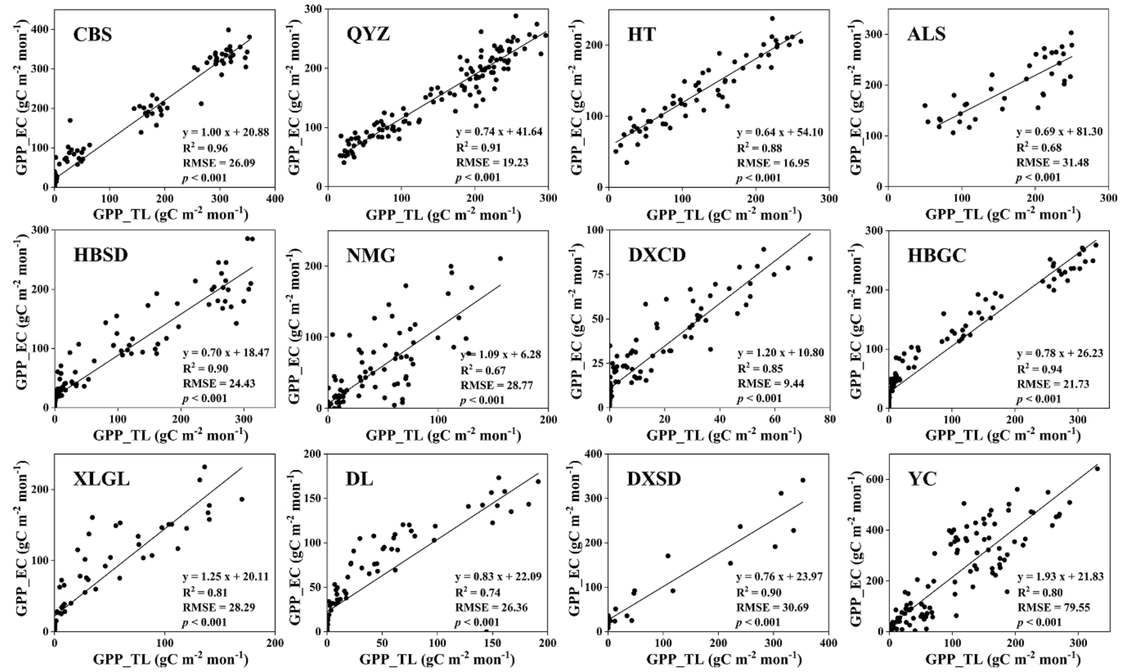

Figure 2. Monthly scale comparison of flux station observed GPP (GPP_EC) and TL-LUE simulated GPP (GPP_TL).

an average R^2 of 0.80 in 99.40% of the vegetation areas.

3.2. The spatial distributions of annual mean GPP and its impacting factors

Figure 3(a) shows the spatial distribution of the annual mean GPP from 2001 to 2020 in the eight engineering areas. Overall, GPP showed a clear gradient of low to high form the north to the south. Among these areas, the highest annual GPP was in Area VII (1927.19 g C m^{-2} yr^{-1}), followed by Area VIII (1502.15 g C m^{-2} yr^{-1}) and in Area VI (1288.57 g C m^{-2} yr^{-1}). The lowest annual GPP was in Area IV (629.81 g C m^{-2} yr^{-1}) and Area I (479.03 g C m^{-2} yr^{-1}).

In general, LCC and CO_2 fertilizations have positively impacted the GPP over the eight areas (figures 3(b) and (c)). The largest impacts of LCC on GPP were mainly in northeast and southern China (figure 3(b)). The impact of CO_2 fertilization on GPP varies significantly in spatial distribution, decreasing from the southeast coast to the northwest inland. The largest impacts were mainly in southern China, with the impact on GPP up to 30 g C m^{-2} yr^{-1}, while the least impacts were mainly in southwest, northwest and north China, with less than 3 g C m^{-2} yr^{-1}(figure 3(c)).

Differently, the climate factors have both negative and positive effects over different engineering areas, mostly playing negative roles (figures 3(d)–(f)). Most vegetation GPP was negatively affected by Rad variations, with the largest impacts exceeding −100 g C m^{-2} yr^{-1}, mainly in Northeast and Central China. Only a small proportion of vegetation GPP was positively affected by Rad variations, mainly in the south-west China (figure 3(d)). In addition, the positive effect of Ta change on GPP locates in the high GPP areas which exceed 15 g C m^{-2} yr^{-1} except the Sichuan Basin (figure 3(e)). Notably, the GPP in areas VI and VII were weakened by VPD changes most strongly (figure 3(f)).

3.3. Long-term trends of annual GPP and contributions of LCC and CO_2 fertilizations over different engineering areas

Firstly, the annual total GPP and long-term trends in the eight areas from 2001 to 2020 were analyzed (figures 4(a) and (b)). Among these areas, the largest total annual GPP locates at Area VI, which has an average of 1.49 Pg C yr^{-1}. This is mainly because, Area VI is located in the south of China, where has abundant forest and grassland with vegetation-friendly climatic environment. This area also has the largest increasing trend, with a value of 0.0106 Pg C yr^{-2}. In terms of total annual GPP, it was followed by Area VII (0.53 Pg C yr^{-1}) and Area I (0.50 Pg C yr^{-1}). The mean total annual GPP in Area I was slightly lower than that in Area VII, but the growth rate was higher (0.0065 and 0.0078 Pg C yr^{-2}, respectively), resulting in a decreased difference in total annual GPP over time. In comparison, areas VIII, V, IV, III and II had relatively low annual GPP and trends. We further analyzed the contributions of total annual GPP by different vegetation types (supplementary figure S2(a)). The average annual GPP for forest, cropland, and grasslands for each area were ranged from 1.97 × 10^6 to 4.96 × 10^8, from 5.09 × 10^7 to 3.23 × 10^8, and from 3.35 × 10^7 to 1.38 × 10^9 T C yr^{-1}, respectively.

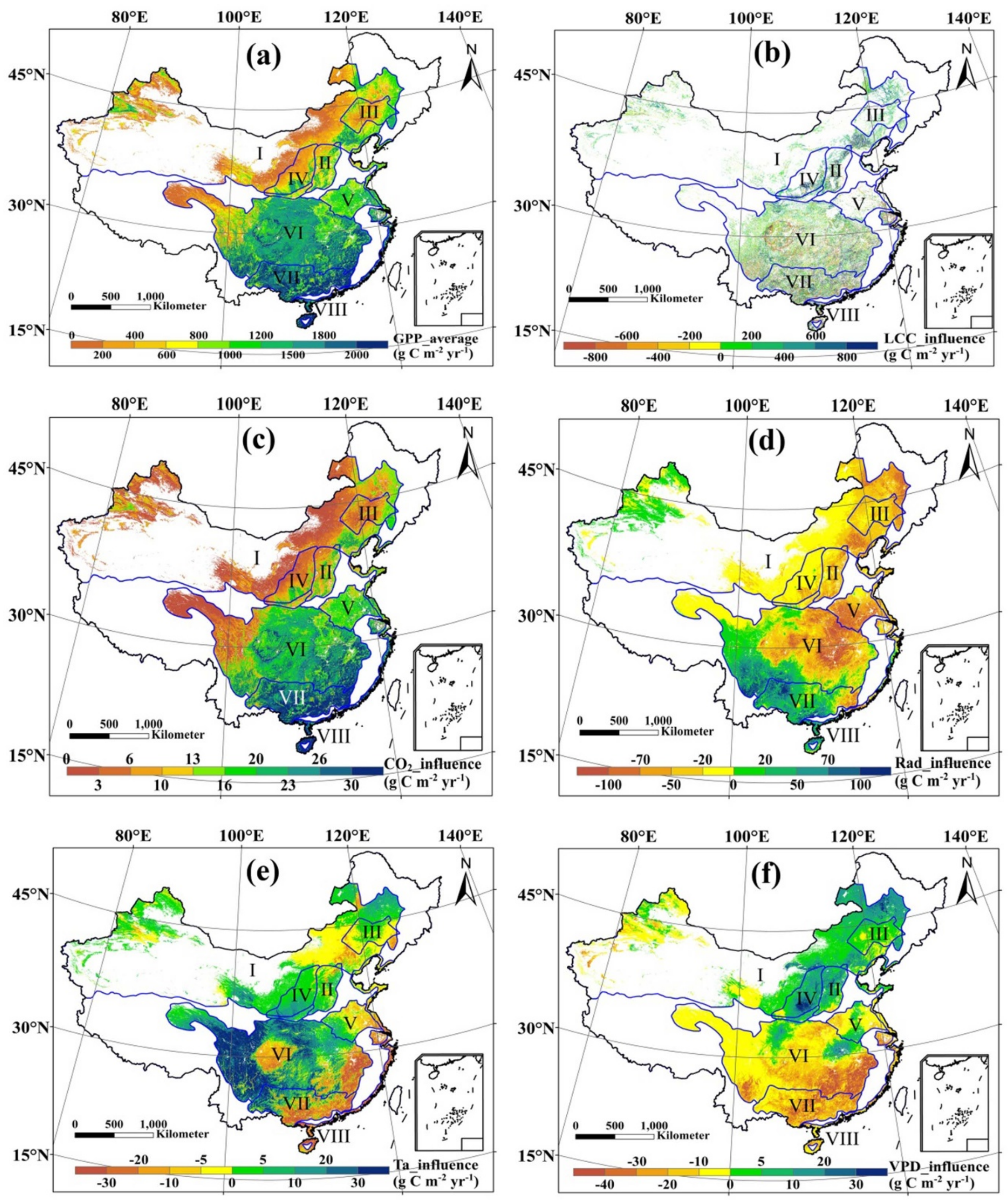

Figure 3. Spatial distribution of mean GPP in eight areas in China from 2001 to 2020 (a), and spatial distribution of annual mean value of impact of LCC (b), CO_2 (c), Rad (d), Ta (e) and VPD (f) on GPP from 2001 to 2020.

Then, the impacts of LCC on GPP in the eight areas during 2001–2020 were investigated (figures 4(c) and (d)). Overall, the areas VI, I and VII were subjected to higher impacts of LCC on GPP, with average values of 22.50, 18.46, 17.04 and 18.82 Tg C yr^{-1}, respectively. Their impacts were also significantly increased, with 3.26, 2.59 and 3.06 Tg C yr^{-2}, respectively. This was followed by the areas IV and II (7.77 and 6.76 Tg C yr^{-1}, respectively), whose impacts on GPP were moderately increased (1.13 and 1.02 Tg C yr^{-2}, respectively). It implied that vegetation GPP was less affected by LCC in areas IV and II, albeit that GPP was affected by higher LCC per unit area in areas IV and II. In comparison, the GPP in Area III, VIII and V were less affected by LCC, with averages of 1.98, 0.84 and -1.67 Tg C yr^{-1}, respectively, and trends in total annual impact were 0.34, 0.28 and -0.22 Tg C yr^{-2}, respectively. The impact of LCC on average annual GPP for forest, cropland, and grasslands for each area were ranged from 1.05×10^5 to 1.18×10^7, from -1.77×10^6 to 4.02×10^7, and from 7.42×10^5 to 1.29×10^7 T C yr^{-1}, respectively (supplementary figure S2(b)).

Lastly, the impacts of CO_2 changes on GPP in the eight areas during 2001–2020 were investigated (figures 4(e) and (f)). The GPP in Area VI affected by CO_2 changes during 2001–2020 was relatively higher, with an average value of 20.10 Tg C yr^{-1}. Its

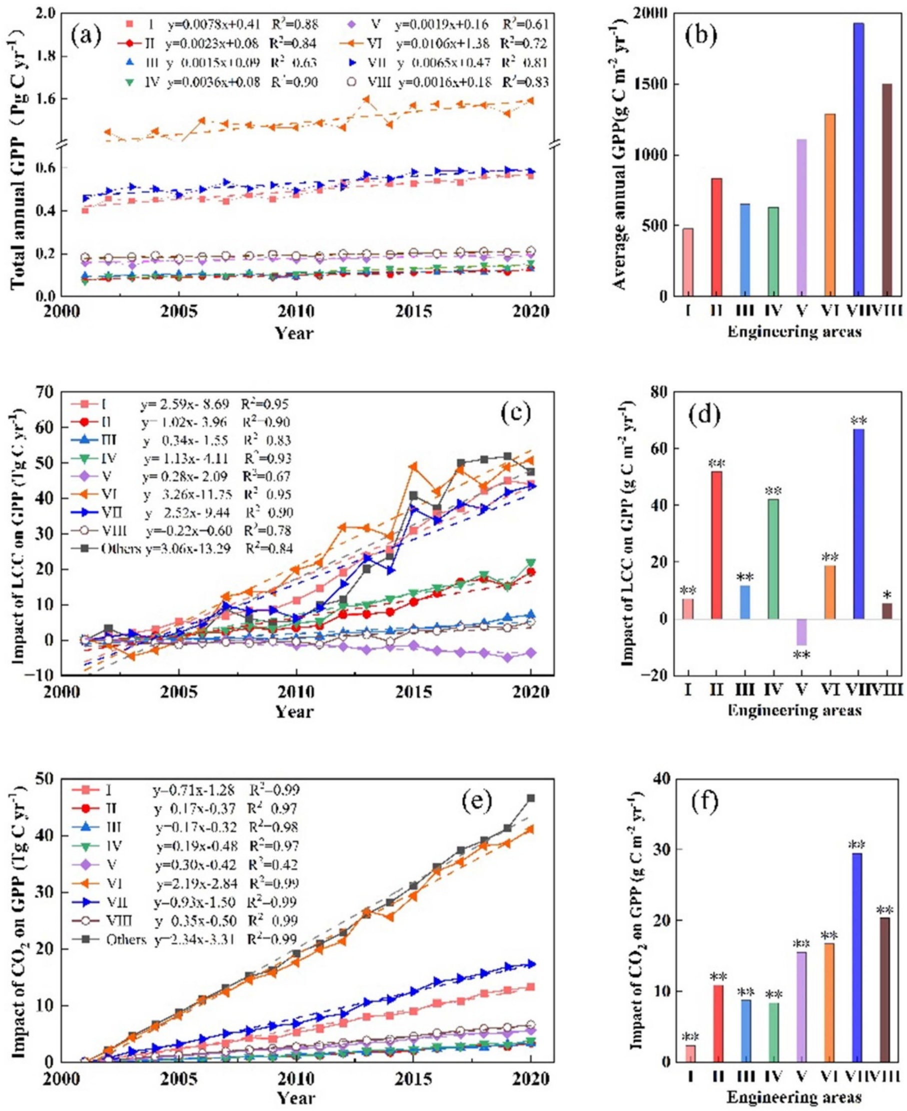

Figure 4. Long-term trend of the annual GPP (a) and that of the contributions of LCC (c) and CO_2 (e) on GPP, and average value of vegetation GPP per unit area (b) and the impact of LCC (d) and CO_2 (f) change on GPP per unit area in eight areas from 2001 to 2020. T-test was used to analyze the significance of the different factors on GPP variations. The symbols '**' and '*' represent significance levels at $p < 0.01$ and $0.05 < p < 0.01$, respectively.

increasing trend of the impact was also high, with 2.34 Tg C yr^{-2}. It was followed the areas VII and I, with means of 8.29 and 6.19 Tg C yr^{-1}, respectively. However, the increasing trends were moderate, at 0.93 and 0.71 Tg C yr^{-2}, respectively, which showed that the GPP in areas VII and I was positively affected by lower CO_2 changes. In comparison, the GPP in areas VIII, V, IV, III and II were minimally affected by CO_2 changes, with averages of 3.13, 2.75, 1.55, 1.48 and 1.42 Tg C yr^{-1}, respectively, and the increasing trends of annual sums of impacts were low, with 0. 35, 0.30, 0.19, 0.17 and 0.17 Tg C yr^{-2}, respectively. The impact of CO_2 changes on average annual GPP for forest, cropland, and grasslands for each area were ranged from 2.80×10^{4}–6.00×10^{6}, from 4.92×10^{5}–1.88×10^{7}, and from 7.19×10^{5}–4.91×10^{6} T C yr^{-1} (supplementary figure S2(c)).

3.4. Impact of the change of climate factors on long-term GPP over different engineering areas

The impact of the changes of different climate factors (i.e. radiation, air temperature, and VPD) on long-term GPP over different engineering areas were investigated. Firstly, we analyzed the impact of radiation change on GPP (figures 5(a) and (b)). It shows that the GPP in areas I and VI were negatively affected by Rad changes during 2001–2020, with the averages of −19.31, −18.5 and −36.27 Tg C yr^{-1}, respectively, and the increasing trends of the negative impacts were −1.81, −1.00 and −1.14 Tg C yr^{-2}. Areas V, III, II, IV and VIII were subject to low total annual GPP impacts of Rad changes, with 20 year averages of −9.31, −5.46, −4.31, −2.60 and −1.65 Tg C yr^{-1}, respectively, and the trends of the impact were not statistically significant, with 0.13, −0.19, −0.03, −0.12

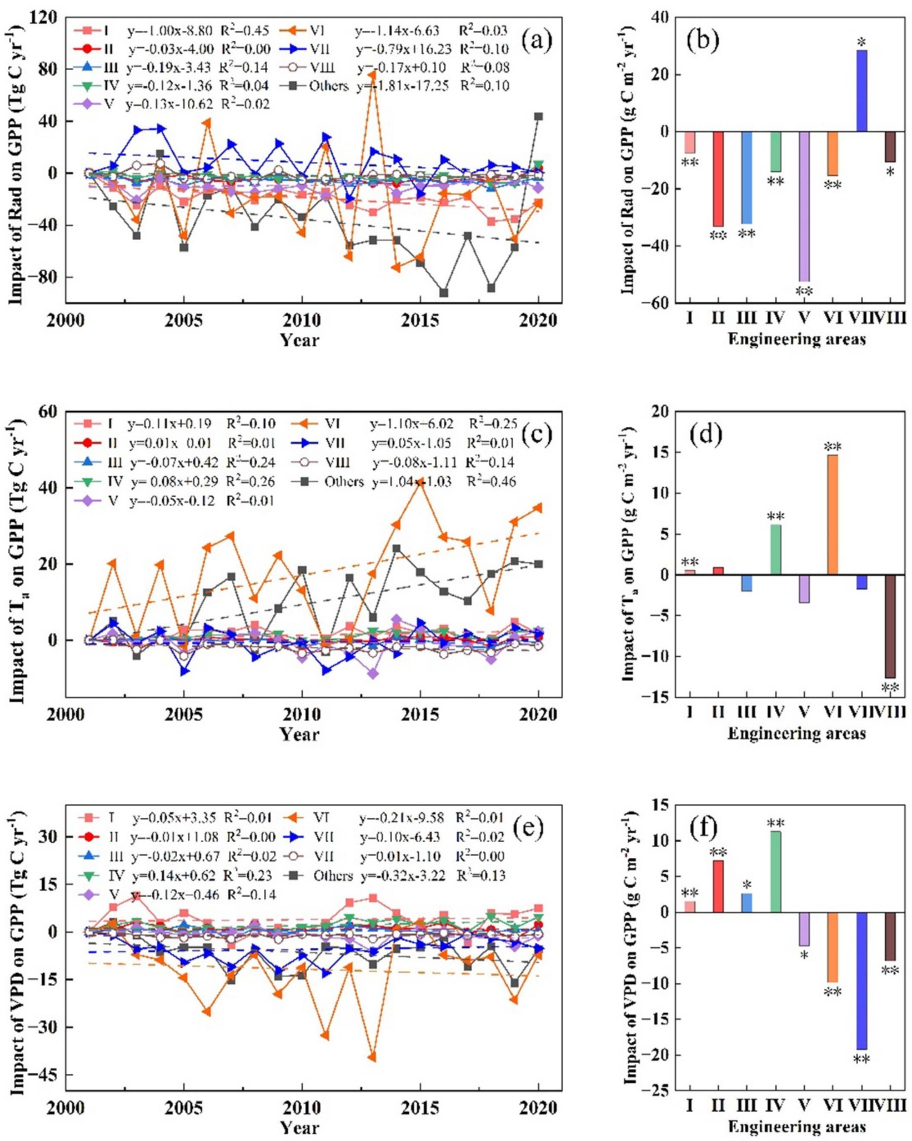

Figure 5. Long-term trend of the annual impact of Rad (a), Ta (c) and VPD (e) on GPP, and the impact of change of Rad (b), Ta (d) and VPD (f) on GPP per unit area in eight areas from 2001 to 2020. T-test was used to analyze the significance of the different factors on GPP variations. The symbols '**' and '*' represent significance levels at $p < 0.01$ and $0.05 < p < 0.01$, respectively.

and -0.17 Tg C yr^{-2}, respectively. Area VII was positively influenced by Rad changes on GPP, and the 20 year mean value of the positive influence was 7.98 Tg C yr^{-1}, with a trend of -0.79 Tg C yr^{-2}. The impact of Rad variations on average annual GPP for forest, cropland, and grasslands for each area were ranged from -6.90×10^5–1.89×10^6, from -1.61×10^7–9.51×10^6, and from -1.18×10^7–1.05×10^6 T C yr^{-1} (supplementary figure S2(d)).

Then, we analyzed the impact of Ta on GPP (figures 5(c) and (d)). It shows that Ta changes had a positive effect on GPP in Area VI from 2001 to 2020, with 20 year mean values of 17.60 and 9.87 Tg C yr^{-1}, respectively, and the increasing trends of the impact were slightly higher, with 1.04 and 1.10 Tg C yr^{-2}, respectively. The GPP in areas I, IV and II were affected by Ta changes with relatively low total annual values of 1.36, 1.13 and 0.12 Tg C yr^{-1}, respectively, and the increasing trends of the impact were relatively low at 0.11, 0.08 and 0.01 Tg C yr^{-2}, respectively, showing that the vegetation GPP in areas I, IV and III were less affected by Ta changes. Areas VIII, V, VII and III were negatively affected by Ta changes on GPP, with 20 year means of -1.95, -0.60, -0.49 and -0.33 Tg C yr^{-1}, respectively, but the trends of the impact were not prominent, at -0.08, -0.07 and $-0.$ 07 Tg C yr^{-2} respectively. The impact of Rad variations on average annual GPP for forest, cropland, and grasslands for each area were ranged from -2.38×10^5–7.35×10^6, from -1.71×10^6–1.95×10^7, and from -9.55×10^5–7.61×10^5 T C yr^{-1} (supplementary figure S2(e)).

Lastly, we analyzed the impact of VPD on GPP (figures 5(e) and (f)). It shows that the GPP in areas VI and VII were negatively affected by VPD changes during 2001–2020, and the total annual value of

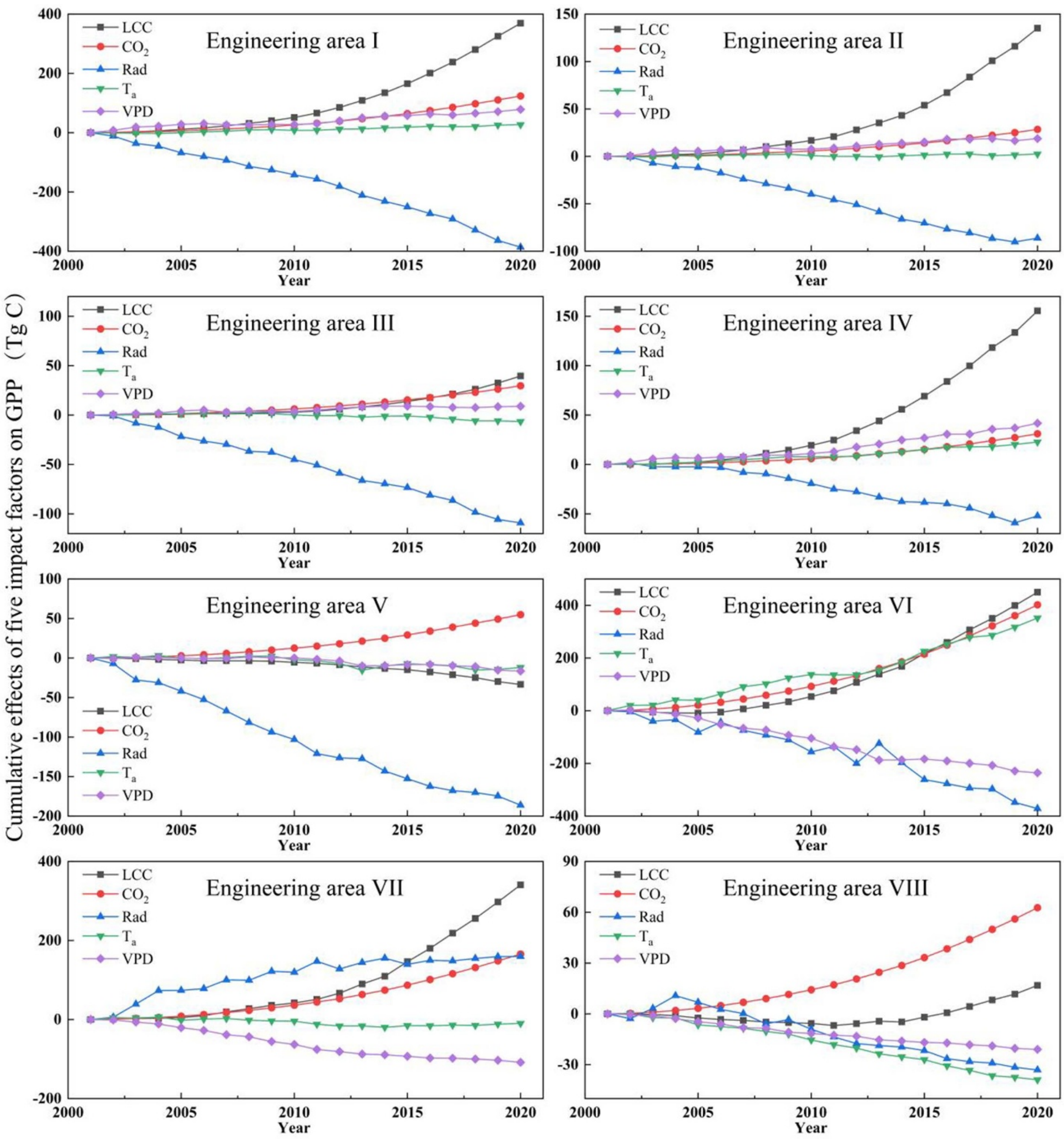

Figure 6. Cumulative effects of five impact factors (LCC, CO_2, Rad, Ta and VPD) on GPP in eight areas from 2001 to 2020.

negative impact was obvious, with 20 year mean values of −11.80 and −5.41 Tg C yr^{-1}, respectively. The trend of total annual impact was also more pronounced, with −0.32, and −0.21 Tg C yr^{-2}, suggesting that vegetation GPP was more negatively affected by changes in VPD. In areas VIII and V, GPP were negatively impacted by changes in VPD, with the 20 year annul mean values of −1.05 and −0.83 Tg C yr^{-1}, respectively. In areas I, IV, II and III, GPP were positively affected by changes in VPD, with 20 year means of positive impacts of 3.93, 2.08, 0.94 and 0.44 Tg C yr^{-1}, respectively. The impact of VPD variations on average annual GPP for forest, cropland, and grasslands for each area were ranged from -2.47×10^6–3.72×10^5, from -1.37×10^7–3.44×10^6, and from -1.50×10^6–1.04×10^6 T C yr^{-1} (supplementary figure S2(f)).

3.5. Cumulative impact of impact factors on vegetation GPP during 2000–2020

The cumulative impact of changes in LCC, CO_2, Rad, Ta and VPD on GPP during 2001–2020 were analyzed for the eight areas (figure 6 and table 3). In Area I, LCC mainly dominated the increase in GPP, with a cumulative effect of up to 369.16 Tg C by 2020. In contrast, CO_2, VPD and T_a have a comparatively lower positive cumulative impact on GPP. However, the positive effects of the LCC, CO_2, Ta and VPD changes on GPP were offset by 2012 as a result of the Rad changes, which had a cumulative effect of −386.21 Tg C on GPP. Similarly, in Area II, LCC mainly dominated the increase in GPP, with a cumulative effect of up to 135.20 Tg C by 2020. CO_2, VPD and Ta had the lowest cumulative impact on GPP with 28.47, 18.77 and 2.47 Tg C respectively, contributing

Table 3. Cumulative impact of five impact factors on GPP in eight areas from 2001 to 2020.

Aare	LCC (Tg C)	CO_2 (Tg C)	Rad (Tg C)	Ta (Tg C)	VPD (Tg C)
I	369.16	123.83	−386.21	27.27	78.59
II	135.20	28.47	−86.22	2.47	18.77
III	39.54	29.59	−109.15	−6.53	8.90
IV	155.50	31.06	−52.09	22.67	41.68
V	−33.47	54.94	−186.12	−11.97	−16.55
VI	449.94	401.98	−371.46	351.96	−235.98
VII	340.83	165.77	159.65	−9.85	−108.30
VIII	16.84	62.69	−20.97	−33.10	−38.91

only 21.05%, 13.88% and 1.83% to the cumulative impact of LCC. Conversely, GPP was negatively affected by Rad changes with a cumulative effect of −86.22 Tg C. The positive effects of LCC, CO_2, Ta and VPD changes on GPP were completely offset by 2013. In Area III, the Rad variation mainly dominated the decrease in GPP, with a negative cumulative effect of up to −109.15 Tg C by 2020. The cumulative effect of Ta on GPP was also negative. In Area IV, LCC mainly dominated the increase in GPP, with a cumulative impact of up to 155.50 Tg C by 2020. VPD, CO_2 and Ta have the lower cumulative impact on GPP. Conversely, GPP was negatively affected by changes in Rad with a cumulative impact of −52.09 Tg C. In Area V, Rad variation dominated the GPP reduction, with a negative cumulative effect of up to −186.12 Tg C by 2020. Meanwhile, the cumulative effects of LCC, VPD and Ta on GPP are also negative, at −33.47 Tg C, −16.55 Tg C and −11.97 Tg C respectively. On the contrary, only CO_2 had a positive cumulative effect on GPP of 54.94 Tg C. In area VI, LCC, CO_2 and Ta changes dominated the increase of GPP with cumulative effects up to 449.94, 401.98 and 351.96 Tg C by 2020. Until 2012, Ta changes played a decisive role in the cumulative effect of GPP, followed by CO_2 and LCC, while the dominance of LCC gradually stabilized only after 2017. In particular, changes in Rad and VPD had a negative impact on GPP, with cumulative effects of −371.46 and −235.98 Tg C. In fact, each impact factor significantly changed the GPP of the vegetation in Area VI. In area VII, GPP was mainly positively influenced by Rad until 2015, while LCC replaced Rad to dominate the increase in GPP after 2015, and the cumulative effect of CO_2 also exceeded Rad for the first time by 2020. The cumulative effect of LCC on GPP in 2020 was calculated to be as high as 340.83 Tg C, followed by CO_2 and Rad with 165.77 and 159.65 Tg C, respectively. Similarly, Ta and VPD have negative cumulative effects on GPP with −9.85 and −108.30 Tg C, respectively. In area VIII, LCC dominated the increase in GPP before 2006, while the cumulative effect of land use changes on GPP decreased dramatically after 2006, and CO_2 took over as the main driver of GPP growth, with a cumulative effect of up to 62.69 Tg C by 2020. The cumulative effect of LCC on GPP was also favourable at 16.84 Tg C. The combined cumulative impact of Ta, Rad and VPD on GPP was negative at −38.91, −33.10 and −20.97 Tg C, respectively.

4. Discussions

4.1. LCC accelerated GPP increase in most areas

With various transformation modes, LCC accelerated GPP increase in most forestry engineering areas. In Area I, the greening area had largely increased since 1978 and a large portion of grasslands and wastelands in Northeast China has been converted to croplands (Ye *et al* 2009). In Area II, the area for grasslands and croplands had increased clearly since 2001, contributing to a large positive influence of LCC on GPP (figure 3 and supplementary figure S3). In Area III and IV, the land cover was mainly transformed from grasslands to croplands and forests (figure 4 and supplementary figure S3). In Area V, cropland and forests transformed into grasslands and urban, which resulted to the weak negative effects on GPP. In Area VI and VII, the land cover was mainly transformed from grasslands and cropland to forests. In Area VIII, the land cover was mainly transformed from grasslands and cropland to forests and urban, which is located in the eastern part of China, and the rapid urbanization in the past 20 years has offset partially the positive impacts of LCC.

The important role of LCC on GPP changes was also found in the three northern regions over 1982–2017 (Xie *et al* 2020), with the fallowing program (Feng *et al* 2016) and the grazing program (Gang *et al* 2018) preventing grassland degradation and contributing more than 1 g C m^{-2} yr^{-1} to GPP trends. Zhang *et al* (2022) found that in a study of Area VII for nearly 20 years, the positive impact of LCC on GPP also increased rapidly after 2010 due to the increase in the number of plantation forests and the rapid growth of new plantation forests (Zhang *et al* 2014, Tong *et al* 2018). Li *et al* (2017) found that human activities in Area IV were the main influencing factor of vegetation change, with a contribution of 55% and over 60% in some areas. The impact of LCC on GPP has shown a highly remarkable increasing trend over the past 20 years, indicating that ecological conservation policies in China have made great progress in restoring degraded forests and increasing vegetation productivity despite the adverse effects of urbanization (Chen *et al* 2021, Yue *et al* 2021).

4.2. Radiation variation decreased GPP in most areas

Rad variation weakened GPP in the eight engineering areas, except Area VII, with a decreasing trend, in line with the finding by Chen *et al* (2021) for the study area of China. In Area I, which locates in northern China, the impact of Rad showed a decreasing trend since 2001 (supplementary figure S4), and vegetation GPP was positively correlated with PAR (Piao *et al* 2006), so this area was increasingly negatively affected by Rad variation. Similarly, the northeastern part of Area VI is the area with strong Rad reduction (figure 4), and the negative effect of Rad change on GPP per unit area exceeds -100 g C m^{-2} yr^{-1} (figure 4), making Area VI more negatively affected by Rad change. Area VII is located in southern China with a warm and humid climate and limited Rad due to cloud cover (Li *et al* 2017, Feng and Wang 2019). Enhanced Rad after 2001 led to a longer growing season, which increased vegetation GPP (Sun *et al* 2018). In addition, cloud cover increased the scattered Rad ratio and thus enhances LUE (Gu *et al* 2003, Rap *et al* 2018), which is more conducive to improving vegetation productivity (Zhou *et al* 2020), making Rad changes promote vegetation GPP in Area VII (Zhang *et al* 2022).

4.3. Regulations of Ta and VPD on GPP inter-annual fluctuation

The response of vegetation GPP to Ta is complex, since warming extends the vegetation growth period (Keenan *et al* 2014), but increases water stress (Reich *et al* 2018) that inhibiting GPP as well. The annual total impact of Ta changes on GPP and its trend varied widely across different regions. Compared with other factors, GPP was more influenced by Ta changes in Area VI, which was in line with the findings by Qu *et al* (2018) and Ye *et al* (2020). Ta has generally increased in the Yangtze River basin since 2001, which accelerated land carbon uptake (Farquhar *et al* 1980, Piao *et al* 2013), and the positive effect of Ta change on GPP is high. Although Area I has the largest area among the eight areas, it is located in northwestern China and is more restricted by water, which still increases slightly in the context of increasing desertification (Wang *et al* 2010), benefiting from human intervention and management (Xie *et al* 2020). Area I, IV, II and III are located in severe water shortage areas, where decreased VPD had a positive effect on vegetation productivity (Tuo *et al* 2018), coinciding with the finding by Xie *et al* (2020). The increased VPD in Area VI lead to the negative impact on GPP, which was consistent with the finding by Ye *et al* (2020).

4.4. Uncertainties of this study

Some uncertainties exist in this study. Firstly, the CO_2 concentration data used in this study for 2001–2020 are monthly averaged CO_2 data measured at the Mauna Loa Observatory in Hawaii, with the same value of CO_2 concentration for each month globally. However, the CO_2 concentration actually varies in time and space, and such treatment could lead to uncertainty when disentangling the effect of CO_2 on GPP. Secondly, the TL-LUE model does not take into account the effects of nitrogen deposition and tree age, which would lead to the inability to quantitatively explore the effects of these factors on GPP. Stand age has a non-linear relationship with forest carbon sink (Zhou *et al* 2015). Although some studies reported that the increasing hydraulic limitations would reduce GPP in aging forest (Drake *et al* 2011), and some suggested that triose phosphate utilization limitation would lead to decrease of GPP (Barnard and Ryan 2003), till now it lacks of sufficient observations to quantifying the effects of tree age in GPP. Therefore, in future studies, the perturbation functions of other influencing factors should be incorporated in the model to facilitate such attribution studies. Thirdly, leaf angle should change with vegetation types, but there was no dataset for depicting the spatial distributions of leaf inclination angles, so the mean leaf inclination angle as 60 degrees was used in this study, which could lead to some uncertainties of GPP estimation. Fourthly, the approach used to scale up input variables from instantaneous to daily scales by simply averaging them may lead to some uncertainties in GPP simulation. In addition, topography affects the surface solar radiation, as terrain shading can reduce direct radiation, and diffuse radiation can be amplified due to reflected flux from surrounding terrain (Wang *et al* 2018, Zhang *et al* 2019), which further affect the GPP dynamics. In this study, the effects of topography on GPP variations were not considered, which should be paid attention in future studies, especially for mountainous areas.

5. Conclusions

In this study, we disentangled the roles of LCC, CO_2 fertilization, and climate changes on GPP in the eight forestry engineering areas during 2001–2020 using the TL-LUE model with scenario simulations. The main findings are:

(1) Among the eight areas, LCC attributed from the forestry engineering initiatives greatly accelerated the increase of GPP in seven areas except Area V, in which cropland and forests transformed into grasslands and urban, resulting to the weak negative effects on GPP. In addition, CO_2 fertilization played a near-equivalent role as LCC in all areas.

(2) Rad changes decreased the GPP in seven areas due to the decrease of radiation during 20 years, except Area VII. In Area VII, the increased radiation led to the positive effect on GPP.
(3) The increased VPD in the areas V, VI, VII and VIII affected the GPP negatively and the decreased VPD in the other four areas impacted the GPP positively. Compared with other areas, GPP in Area VI was more influenced by Ta changes.

These findings could improve our understanding of the contribution of China's afforestation on its forest productivity in a changing climate, which may help to better manage forests to tackle the challenge of the climate crisis in the future.

Data availability statements

The MODIS land cover data were MCD12Q1 v006 from https://lpdaac.usgs.gov/products/mcd12q1v006/. FluxSat GPP and GOSIF GPP data were obtained from the website https://avdc.gsfc.nasa.gov/pub/tmp/FluxSat_GPP/ and http://globalecology.unh.edu/data/GOSIF-GPP.html. The boundary data for the eight forest engineering data were from www.resdc.cn/data.aspx?DATAID=138.

All data that support the findings of this study are included within the article (and any supplementary files).

Acknowledgments

This study was funded by the National Key Research and Development Program of China (2019YFA0606604), National Natural Science Foundation of China (Nos. 42277453 and 42077419). We acknowledge China Meteorological Administration for providing in-situ meteorological data. We sincerely acknowledge Ronggao Liu and Yang Liu from the Institute of Geographical Sciences and Natural Resource Research of Chinese Academy of Sciences for providing the GLOBMAP LAI v3 data product. We sincerely acknowledge the ChinaFLUX team and data collectors for sharing these valuable in-situ flux data. We also sincerely acknowledge Joanna Joiner from NASA Goddard Space Flight Center for providing the FluxSat GPP product and Jingfeng Xiao from New Hampshire University for providing the GOSIF GPP product.

ORCID iDs

Yanlian Zhou https://orcid.org/0000-0002-9293-0365
Wei He https://orcid.org/0000-0003-0779-2496
Ngoc Tu Nguyen https://orcid.org/0000-0003-3251-1799
Weimin Ju https://orcid.org/0000-0002-0010-7401

References

Ahlström A *et al* 2015 The dominant role of semi-arid ecosystems in the trend and variability of the land CO_2 sink *Science* **348** 895–9
Anderegg W R L *et al* 2015 Pervasive drought legacies in forest ecosystems and their implications for carbon cycle models *Science* **349** 528–32
Bai Y, Liang S L and Yuan W P 2021 Estimating global gross primary production from sun-induced chlorophyll fluorescence data and auxiliary information using machine learning methods *Remote Sens.* **13** 20
Barnard H and Ryan M 2003 A test of the hydraulic limitation hypothesis in fast-growing Eucalyptus saligna *Plant Cell Environ.* **26** 1235–45
Bi W, He W, Zhou Y, Ju W, Liu Y, Liu Y, Zhang X, Wei X and Cheng N 2022 A global 0.05° dataset for gross primary production of sunlit and shaded vegetation canopies from 1992 to 2020 *Sci. Data* **9** 213
Byrne B *et al* 2021 The carbon cycle of southeast Australia during 2019–2020: drought, fires, and subsequent recovery *AGU Adv.* **2** 20
Chen J M, Ju W, Ciais P, Viovy N, Liu R, Liu Y and Lu X 2019 Vegetation structural change since 1981 significantly enhanced the terrestrial carbon sink *Nat. Commun.* **10** 4259–7
Chen J M, Liu J, Cihlar J and Goulden M L 1999 Daily canopy photosynthesis model through temporal and spatial scaling for remote sensing applications *Ecol. Modell.* **124** 99–119
Chen S Y, Zhang Y L, Wu Q L, Liu S H, Song C H, Xiao J F, Band L E and Vose J M 2021 Vegetation structural change and CO_2 fertilization more than offset gross primary production decline caused by reduced solar radiation in China *Agric. For. Meteorol.* **296** 15
Ciais P *et al* 2005 Europe-wide reduction in primary productivity caused by the heat and drought in 2003 *Nature* **437** 529–33
Deng F, Chen J M, Plummer S, Chen M Z and Pisek J 2006 Algorithm for global leaf area index retrieval using satellite imagery *IEEE Trans. Geosci. Remote Sens.* **44** 2219–29
Drake J, Davis S, Raetz L and DeLucia E 2011 Mechanisms of age-related changes in forest production: the influence of physiological and successional changes *Glob. Change Biol.* **17** 1522–35
Fang J Y, Guo Z D, Hu H F, Kato T, Muraoka H and Son Y 2014 Forest biomass carbon sinks in East Asia, with special reference to the relative contributions of forest expansion and forest growth *Glob. Change Biol.* **20** 2019–30
Farquhar G D, Caemmerer S V and Berry J A 1980 A biochemical-model of photosynthetic CO_2 assimilation in leaves of c-3 species *Planta* **149** 78–90
Feng F and Wang K C 2019 Determining factors of monthly to decadal variability in surface solar radiation in China: evidences from current reanalyses *J. Geophys. Res.-Atmos.* **124** 9161–82
Feng X *et al* 2016 Revegetation in China's Loess Plateau is approaching sustainable water resource limits *Nat. Clim. Change* **6** 1019–22
Friedlingstein P *et al* 2010 Update on CO_2 emissions *Nat. Geosci.* **3** 811–2
Gang C C, Zhao W, Zhao T, Zhang Y, Gao X R and Wen Z M 2018 The impacts of land conversion and management measures on the grassland net primary productivity over the Loess Plateau, Northern China *Sci. Total Environ.* **645** 827–36
Gu L H, Baldocchi D D, Wofsy S C, Munger J W, Michalsky J J, Urbanski S P and Boden T A 2003 Response of a deciduous forest to the Mount Pinatubo eruption: enhanced photosynthesis *Science* **299** 2035–8

Guo Z D, Hu H F, Li P, Li N Y and Fang J Y 2013 Spatio-temporal changes in biomass carbon sinks in China's forests from 1977 to 2008 *Sci. China-Life Sci.* **56** 661–71

Hasan S, Shi W Z, Zhu X L and Abbas S 2019 Monitoring of land use/land cover and socioeconomic changes in South China over the last three decades using landsat and nighttime light data *Remote Sens.* **11** 23

He M Z *et al* 2013 Development of a two-leaf light use efficiency model for improving the calculation of terrestrial gross primary productivity *Agric. For. Meteorol.* **173** 28–39

Ichii K, Hashimoto H, Nemani R and White M 2005 Modeling the interannual variability and trends in gross and net primary productivity of tropical forests from 1982 to 1999 *Glob. Planet. Change* **48** 274–86

Jiang C and Ryu Y 2016 Multi-scale evaluation of global gross primary productivity and evapotranspiration products derived from Breathing Earth System Simulator (BESS) *Remote Sens. Environ.* **186** 528–47

Joiner J, Yoshida Y, Zhang Y, Duveiller G, Jung M, Lyapustin A, Wang Y J and Tucker C J 2018 Estimation of terrestrial global gross primary production (GPP) with Satellite data-driven models and eddy covariance flux data *Remote Sens.* **10** 38

Keenan T F *et al* 2014 Net carbon uptake has increased through warming-induced changes in temperate forest phenology *Nat. Clim. Change* **4** 598–604

Li J J, Peng S Z and Li Z 2017 Detecting and attributing vegetation changes on China's Loess Plateau *Agric. For. Meteorol.* **247** 260–70

Li J 2021 A simulation approach to optimizing the vegetation covers under the water constraint in the Yellow River Basin *For. Policy Econ.* **123** 10

Li X and Xiao J F 2019 A global, 0.05-degree product of solar-induced chlorophyll fluorescence derived from OCO-2, MODIS, and reanalysis data *Remote Sens.* **11** 24

Li Z, Chen Y, Li W, Deng H and Fang G 2015 Potential impacts of climate change on vegetation dynamics in Central Asia *J. Geophys. Res. Atmos.* **120** 12345–56

Liu Y B, Xiao J F, Ju W M, Xu K, Zhou Y L and Zhao Y T 2016 Recent trends in vegetation greenness in China significantly altered annual evapotranspiration and water yield *Environ. Res. Lett.* **11** 14

Liu Y, Fu B J, Lu Y H, Wang Z and Gao G Y 2012a Hydrological responses and soil erosion potential of abandoned cropland in the Loess Plateau, China *Geomorphology* **138** 404–14

Liu Y, Liu R G and Chen J M 2012b Retrospective retrieval of long-term consistent global leaf area index (1981–2011) from combined AVHRR and MODIS data *J. Geophys. Res.-Biogeosci.* **117** 14

Liu Z Y *et al* 2019 Global divergent responses of primary productivity to water, energy, and CO_2 *Environ. Res. Lett.* **14** 11

Nemani R R, Keeling C D, Hashimoto H, Jolly W M, Piper S C, Tucker C J, Myneni R B and Running S W 2003 Climate-driven increases in global terrestrial net primary production from 1982 to 1999 *Science* **300** 1560–3

Piao S L, Ciais P, Friedlingstein P, de Noblet-ducoudre N, Cadule P, Viovy N and Wang T 2009 Spatiotemporal patterns of terrestrial carbon cycle during the 20th century glob *Biogeochem. Cycle* **23** 16

Piao S L, Fang J Y and He J S 2006 Variations in vegetation net primary production in the Qinghai-Xizang Plateau, China, from 1982 to 1999 *Clim. Change* **74** 253–67

Piao S *et al* 2013 Evaluation of terrestrial carbon cycle models for their response to climate variability and to CO 2 trends *Glob. Change Biol.* **19** 2117–32

Qu S, Wang L C, Lin A W, Zhu H J and Yuan M X 2018 What drives the vegetation restoration in Yangtze River basin, China: climate change or anthropogenic factors? *Ecol. Indic.* **90** 438–50

Rap A *et al* 2018 Enhanced global primary production by biogenic aerosol via diffuse radiation fertilization *Nat. Geosci.* **11** 640

Reich P B, Sendall K M, Stefanski A, Rich R L, Hobbie S E and Montgomery R A 2018 Effects of climate warming on photosynthesis in boreal tree species depend on soil moisture *Nature* **562** 263

Schaaf C B *et al* 2002 First operational BRDF, albedo nadir reflectance products from MODIS Remote Sens *Remote Sens. Environ.* **83** 135–48

Sulla-Menashe D, Gray J M, Abercrombie S P and Friedl M A 2019 Hierarchical mapping of annual global land cover 2001 to present: the MODIS Collection 6 Land Cover product *Remote Sens. Environ.* **222** 183–94

Sun W Y, Song X Y, Mu X M, Gao P, Wang F and Zhao G J 2015 Spatiotemporal vegetation cover variations associated with climate change and ecological restoration in the Loess Plateau *Agric. For. Meteorol.* **209** 87–99

Sun Z Y, Wang X F, Yamamoto H, Tani H, Zhong G S, Yin S and Guo E L 2018 Spatial pattern of GPP variations in terrestrial ecosystems and its drivers: climatic factors, CO_2 concentration and land-cover change, 1982–2015 *Ecol. Inform.* **46** 156–65

Tong X W *et al* 2018 Increased vegetation growth and carbon stock in China karst via ecological engineering *Nat. Sustain.* **1** 44–50

Tuo D F, Gao G Y, Chang R Y, Li Z S, Ma Y, Wang S, Wang C and Fu B J 2018 Effects of revegetation and precipitation gradient on soil carbon and nitrogen variations in deep profiles on the Loess Plateau of China *Sci. Total Environ.* **626** 399–411

Wang J H, Hong Y, Gourley J, Adhikari P, Li L and Su F G 2010 Quantitative assessment of climate change and human impacts on long-term hydrologic response: a case study in a sub-basin of the Yellow River, China *Int. J. Climatol.* **30** 2130–7

Wang T, Yan G, Mu X, Jiao Z, Chen L and Chu Q 2018 Toward operational shortwave radiation modeling and retrieval over rugged terrain *Remote Sens. Environ.* **205** 419–33

Xiao H, Wang L, Li H, Chen J and Han Y 2019 Evaluation of ecological service value of East-West combined area based on changes of ecosystem pattern a case study in pearl river-Xijiang River Economic Zone *Bull. Soil Water Conserv.* **39** 252

Xiao J F, Zhou Y and Zhang L 2015 Contributions of natural and human factors to increases in vegetation productivity in China *Ecosphere* **6** 20

Xie S D, Mo X G, Hu S and Liu S X 2020 Contributions of climate change, elevated atmospheric CO_2 and human activities to ET and GPP trends in the Three-North region of China *Agric. For. Meteorol.* **295** 14

Xin Z B, Yu X X, Li Q Y and Lu X X 2011 Spatiotemporal variation in rainfall erosivity on the Chinese Loess Plateau during the period 1956–2008 *Reg. Environ. Change* **11** 149–59

Yang H F, Mu S J and Li J L 2014 Effects of ecological restoration projects on land use and land cover change and its influences on territorial NPP in Xinjiang, China *Catena* **115** 85–95

Ye X C, Liu F H, Zhang Z X, Xu C Y and Liu J 2020 Spatio-temporal variations of vegetation carbon use efficiency and potential driving meteorological factors in the Yangtze River Basin *J. Mt. Sci.* **17** 1959–73

Ye Y, Fang X Q, Ren Y Y, Zhang X Z and Chen L 2009 Cropland cover change in Northeast China during the past 300 years *Sci. China* D **52** 1172–82

Yue X, Zhang T and Shao C 2021 Afforestation increases ecosystem productivity and carbon storage in China during the 2000s *Agric. For. Meteorol.* **296** 108227

Zhang S, Li X, She J and Peng X 2019 Assimilating remote sensing data into GIS-based all sky solar radiation modeling for mountain terrain *Remote Sens. Environ.* **231** 11239

Zhang X Y, Zhou Y L, He W, Ju W M, Liu Y B, Bi W J, Cheng N and Wei X N 2022 Land cover change instead of solar radiation change dominates the forest GPP increase during the recent phase of the Shelterbelt Program for Pearl River *Ecol. Indic.* **136** 13

Zhang Y L, Song C H, Zhang K R, Cheng X L, Band L E and Zhang Q F 2014 Effects of land use/land cover and climate changes on terrestrial net primary productivity in the Yangtze River Basin, China, from 2001 to 2010 *J. Geophys. Res.-Biogeosci.* **119** 1092–109

Zhang Y *et al* 2016 Multiple afforestation programs accelerate the greenness in the 'Three North' region of China from 1982 to 2013 *Ecol. Indic.* **61** 404–12

Zhao M S, Heinsch F A, Nemani R R and Running S W 2005 Improvements of the MODIS terrestrial gross and net primary production global data set *Remote Sens. Environ.* **95** 164–76

Zhao M S and Running S W 2010 Drought-induced reduction in global terrestrial net primary production from 2000 through 2009 *Science* **329** 940–3

Zhou T, Shi P, Jia G, Dai Y, Zhao X, Shangguan W, Du L, Wu H and Luo Y 2015 Age-dependent forest carbon sink: Estimation via inverse modeling *J. Geophys. Res. Biogeosci.* **120** 2473–92

Zhou Y L, Wu X C, Ju W M, Zhang L M, Chen Z, He W, Liu Y B and Shen Y 2020 Modeling the effects of global and diffuse radiation on terrestrial gross primary productivity in china based on a two-leaf light use efficiency model *Remote Sens.* **12** 21

Zhou Y *et al* 2016 Global parameterization and validation of a two-leaf light use efficiency model for predicting gross primary production across FLUXNET sites *J. Geophys. Res. Biogeosci.* **121** 1045–72